Published in final edited form as:
Int J Mass Spectrom. 2017 March ; 414: 80–86. doi:10.1016/j.ijms.2017.01.002.

High-precision analysis of $^{182}W/^{184}W$ and $^{183}W/^{184}W$ by negative thermal ionization mass spectrometry: Per-integration oxide corrections using measured $^{18}O/^{16}O$

Gregory J. Archer[*,1], **Andrea Mundl**, **Richard J. Walker**, **Emily A. Worsham**, and **Katherine R. Bermingham**
Department of Geology, University of Maryland, College Park, MD 20742, USA

Abstract

Here we describe a new analytical technique for the high-precision measurement of $^{182}W/^{184}W$ and $^{183}W/^{184}W$ using negative thermal ionization mass spectrometry (N-TIMS). We improve on the recently reported method of Trinquier et al. (2016), which described using Faraday cup collectors coupled with amplifiers utilizing 10^{13} Ω resistors to continuously monitor the $^{18}O/^{16}O$ of WO_3^- and make per-integration oxide corrections. In our study, we report and utilize a newly measured oxygen mass fractionation line, as well as average $^{17}O/^{16}O$ and $^{18}O/^{16}O$, which allow for more accurate per-integration oxide interference corrections. We also report a Faraday cup and amplifier configuration that allows $^{18}O/^{16}O$ to be continuously monitored for WO_3^- and ReO_3^-, both of which are ionized during analyses of W using Re ribbon. The long-term external precision of $^{182}W/^{184}W$ is 5.7 ppm and 3.7 ppm (2SD) when mass bias corrected using $^{186}W/^{184}W$ and $^{186}W/^{183}W$, respectively. For $^{183}W/^{184}W$ mass bias is corrected using $^{186}W/^{184}W$, yielding a long-term external precision of 6.6 ppm. An observed, correlated variation in $^{182}W/^{184}W$ and $^{183}W/^{184}W$, when mass bias corrected using $^{186}W/^{184}W$, is most likely the result of Faraday cup degradation over months-long intervals.

Keywords

Thermal ionization mass spectrometry; N-TIMS; Tungsten isotope; Oxide interference correction; ^{182}W; ^{183}W

1. Introduction

The short-lived ^{182}Hf-^{182}W isotopic system ($t_{1/2}$ = 8.9 Myr; [2] is useful for constraining the timing of early Solar System metal-silicate equilibration (within the first ~50 Ma of Solar System history) because W is moderately siderophile and largely partitions into Fe-rich metal, whereas Hf is lithophile and partitions entirely into silicate. The most widely used application for this system has been dating core formation of planetary bodies. By measuring W isotopic compositions of iron meteorites, model ages can be calculated,

[*]Corresponding author. archer@uni-muenster.de (G.J. Archer).
[1]Current address: Institut für Planetologie, Westfälische Wilhelms-Universität Münster, Wilhelm-Klemm-Str. 10, 48149 Münster, Germany.

assuming chondritic Hf/W (e.g., [3–5]. The Hf-W isotopic system has also been used to date formation or closure ages of silicate-rich rocks by plotting Hf/W vs. $^{182}W/^{184}W$, yielding internal isochrons. For example, Hf-W isochrons have been used to date formation or closure ages of bulk chondritic meteorites [6], calcium-aluminum-rich inclusions [7], chondrules, and matrix [8]. The ^{182}Hf-^{182}W isotopic system has also been used for terrestrial applications. For example, the W isotopic compositions of mantle-derived rocks have been used to investigate mantle evolution (e.g., [9–13]. In some instances, isotopic variations in $^{182}W/^{184}W$ are <20 ppm.

During the analysis of W by negative thermal ionization mass spectrometry (N-TIMS) when using Re filaments as the ionizing substrate, the different species of ReO_3^- and WO_3^- that incorporate ^{17}O and/or ^{18}O (e.g., $^{182}W^{16}O_2{}^{18}O^-$ and $^{185}Re^{16}O_2{}^{17}O^-$) form isobaric interferences on the signals of some of the primary $W^{16}O_3^-$ beams measured. The oxygen isotopic compositions of ReO_3^- and WO_3^- must, therefore, be accurately determined for isobaric interference corrections, and the in-run fractionation of oxygen isotopes during analyses must also be monitored.

Ref. [14] reported an N-TIMS method capable of measuring $^{182}W/^{184}W$ with a long-term (over a period of 9 months) external reproducibility of <5 ppm (2SD). That study used the oxygen isotopic composition of the atmosphere reported by [15] to make a first-order correction for oxide interferences on primary $^{x}W^{16}O_3^-$ signals. Then, a second-order correction utilized the coevolution of $^{183}W/^{184}W$ and $^{182}W/^{184}W$ to correct for in-run fractionations of oxygen isotopes. Because it used an assumed $^{183}W/^{184}W$ in the correction process, this method did not allow a corresponding measurement of $^{183}W/^{184}W$, which varies among some meteorites (e.g., [7]).

A more recent analytical study [1] reported measurements of both $^{182}W/^{184}W$ and $^{183}W/^{184}W$ with long-term external reproducibilities of ~10–11 ppm (2SD) and ~17–18 ppm (2SD), respectively. As in [14], they corrected minor oxide interferences assuming the atmospheric composition reported by [15]. They corrected in-run fractionations of oxygen isotopes using per-integration measured $^{186}W^{16}O_2{}^{18}O/^{186}W^{16}O_3$ to calculate $^{18}O/^{16}O$ and infer $^{17}O/^{16}O$, using a terrestrial fractionation slope (e.g., [16] passed through the $^{17}O/^{16}O$ and $^{18}O/^{16}O$ reported by [15].

The methods reported by these two prior studies bear some additional scrutiny. The use of the $^{17}O/^{16}O$ and $^{18}O/^{16}O$ ratios reported by [15] may not be appropriate for measurements of ReO_3^- and WO_3^- via N-TIMS. Further, [1] measured only the $^{18}O/^{16}O$ of WO_3^- for each integration. The oxygen isotopic composition of ReO_3^- was assumed to uniformly follow the same evolution trend, which may not be the case. Ref. [1] reported that the method was limited to analyses with Re/W < 0.3, as a systematic bias to higher $^{182}W/^{184}W$ was observed for analyses with high Re/W. Some sample and standard analyses, especially those with low W abundances, sometimes have Re/W > 0.3.

Here we present a new analytical technique, refining the methods of [14] and [1], for making measurements of $^{182}W/^{184}W$ and $^{183}W/^{184}W$ to external precisions ~5 ppm, even for analyses with Re/W > 0.3. This analytical technique uses a newly determined average $^{17}O/$

^{16}O and $^{18}O/^{16}O$, appropriate for measuring ReO_3^- and WO_3^- by N-TIMS, and a new oxygen mass fractionation line for oxide corrections. Per-integration fractionations of oxygen isotopes are corrected for both ReO_3^- and WO_3^- by measuring both $^{186}W^{16}O_2{}^{18}O/^{186}W^{16}O_3$ and $^{187}Re^{16}O_2{}^{18}O/^{187}Re^{16}O_3$.

2. Experimental section

2.1. Filament preparation and loading

A filament loading technique slightly modified from [14] was used. Either 300 ng, 500 ng, or 1000 ng of *Alfa Aesar* W standard solution were loaded onto single Re filaments, which were outgassed ~48 h in advance. Throughout this study, both thick (0.76 mm × 0.030 mm) and thin (0.51 mm × 0.025 mm) Re filaments were used. After loading W, Re filaments were briefly (~1 s) heated to a dull glow, and then left to sit for at least 24 h before loading activator. To enhance ionization, 1 μL of activator solution containing 5 μg each of La and Gd in 5% Teflon distilled HNO_3 was then added in 2–3 aliquots to the standard and sample deposits, and then dried until a white crust formed.

2.2. Instrumental setup

Analyses were performed on the University of Maryland (UMd) *Thermo-Fisher* Triton thermal ionization mass spectrometer. Oxide production was enhanced by bleeding oxygen ($P_{O2} = 1.0 \times 10^{-7}$ mbar) into the source can using a *Varian* leak valve. Similar to the method of [14], all analyses by this study used a multi-static analytical protocol with two lines of acquisition, which allowed Faraday cup biases to be monitored. Each line of acquisition utilized 9 Faraday cups (Table 1). Seven Faraday cups (L4–H2) were electronically connected to amplifiers with 10^{11} Ω resistors, which were electronically rotated during analyses to mitigate amplifier biases. Faraday cups H3 and H4 were connected to amplifiers with 10^{12} Ω resistors to measure the low signals generated by the minor $^{186}W^{16}O_2{}^{18}O^-$ and $^{187}Re^{16}O_2{}^{18}O^-$ species, which were used to calculate per-integration oxide corrections. These amplifiers were not rotated during analyses. The center Faraday cup was centered on masses 232 ($^{184}W^{16}O_3{}^-$) and 234 ($^{186}W^{16}O_3{}^-$) for acquisition lines 1 and 2, respectively.

With this analytical protocol, all $W^{16}O_3{}^-$ and $Re^{16}O_3{}^-$ species were measured, and inter-collector biases were corrected for all major W species ($^{182}W^{16}O_3{}^-$, $^{183}W^{16}O_3{}^-$, $^{184}W^{16}O_3{}^-$, and $^{186}W^{16}O_3{}^-$). The $^{186}W^{16}O_2{}^{18}O^-$ and $^{187}Re^{16}O_2{}^{18}O^-$ species were also measured, from which the $^{18}O/^{16}O$ could be calculated, and the $^{17}O/^{16}O$ could be inferred using an oxygen mass fractionation line. One isotope each of Ta and Os (^{181}Ta and ^{190}Os) were also monitored so that isobaric interference corrections for these elements could be made. However, these signals were below detection limits (a few μV) for all analyses.

Typically, 600 integrations were measured over 770 min, although some analyses were cut short because of rapidly decreasing signals. A 1260 s baseline was measured at the beginning of each analysis and then re-measured every 100 integrations. Each integration consisted of 33.6 s and 8.4 s of acquisition duration for lines 1 and 2, respectively. The idle times before integrations were 10 s and 4 s for acquisition lines 1 and 2, respectively.

2.3. Data reduction

In the first data reduction step, single estimated values (see Section 3.1) for $^{17}O/^{16}O$ (0.0003913) and $^{18}O/^{16}O$ (0.002096) were used to make first-order oxide interference corrections to all $^{x}W^{16}O_3^-$ and $^{x}Re^{16}O_3^-$ signals. Relative abundances of trioxide species for each W and Re isotope (e.g., $^{184}W^{17}O^{16}O_2^-$, $^{184}W^{18}O^{16}O_2^-$, $^{184}W^{18}O_2{}^{16}O^-$, etc.) were calculated following the calculations of [4], using the estimated $^{17}O/^{16}O$ and $^{18}O/^{16}O$. In the next step, first-order oxide-corrected $^{186}W^{16}O_2{}^{18}O^-/^{186}W^{16}O_3^-$ and $^{187}Re^{16}O_2{}^{18}O^-/^{187}Re^{16}O_3^-$ from each integration were used to calculate per-integration $^{18}O/^{16}O$ for WO_3^- and ReO_3^-. A linear trend with a terrestrial fractionation slope (0.0954) that passed through the estimated values for $^{17}O/^{16}O$ (0.0003913) and $^{18}O/^{16}O$ (0.002096) was then used to calculate per-integration $^{17}O/^{16}O$ from each per-integration $^{18}O/^{16}O$.

Per-integration $^{17}O/^{16}O$ and $^{18}O/^{16}O$ were then used to make line-by-line oxide corrections to all $^{x}W^{16}O_3^-$ and $^{x}Re^{16}O_3^-$ signals. All isobaric interferences on $^{x}W^{16}O_3^-$ and $^{x}Re^{16}O_3^-$ for which corrections were made are listed in Table 2. The most signifi-cant isobaric interferences were from $^{x}W^{17}O^{16}O_2^-$, $^{x}W^{18}O^{16}O_2^-$, $xRe^{17}O^{16}O_2^-$, and $^{x}Re^{18}O^{16}O_2^-$species. No corrections were made for low abundance trioxide species (e.g., $^{x}W^{18}O_3^-$) that do not significantly interfere with primary $^{x}W^{16}O_3^-$ and $^{x}Re^{16}O_3^-$ signals Yin, [17]).

Finally, the per-integration oxide-corrected $^{182}W^{16}O_3^-/^{184}W^{16}O_3^-$ were corrected for instrumental mass bias by normalizing to $^{186}W/^{183}W = 0.92767$ or $^{186}W/^{184}W = 1.98594$ [18], using the exponential law [19]. Per-integration oxide corrected $^{183}W^{16}O_3^-/^{184}W^{16}O_3^-$ were only corrected for mass bias using $^{186}W/^{184}W = 1.98594$. Mass bias corrections were calculated using molecular masses (e.g., 232 for $^{184}W^{16}O_3$).

3. Results and discussion

In order to determine the isotopic composition of oxygen associated with Re trioxide formation, we measured the isotopic compositions of Re beams generated by loading activator onto Re filaments with no W. The results of 8 analyses of Re ribbon are summarized in Table 3, and shown in Fig. 1. Using these results, data for 30 analyses of standard solutions (300 ng–1000 ng *Alfa Aesar* W) are summarized in Table 4, and shown in Figs. 2, 3, and 4. A natural sample (group IVB iron meteorite Skookum) analyzed using this method, and compared to previously published results, is shown in Fig. 8.

3.1. First-order and per-integration oxide corrections

High-precision W analyses at the ~5 ppm level require either second-order [14] or per-integration [1] oxide corrections because of in-run mass-dependent oxygen fractionation. This study utilized per-integration oxide corrections because $^{183}W/^{184}W$, which varies nature, can be measured using this method.

Before per-integration oxide corrections could be performed, the signals used to calculate per-integration $^{17}O/^{16}O$ and $^{18}O/^{16}O$ for WO_3^- and ReO_3^- ($^{186}W^{16}O_2{}^{18}O^-$, $^{186}W^{16}O_3^-$, $^{187}Re^{16}O_2{}^{18}O^-$, and $^{187}Re^{16}O_3^-$) had to be first-order oxide-corrected. First-order oxide correction is defined as an oxide correction using a single, assumed value (i.e., an estimated

$^{17}O/^{16}O$ and $^{18}O/^{16}O$). For this estimate, the means of $^{17}O/^{16}O$ and $^{18}O/^{16}O$ calculated from $^{187}Re^{16}O_2{}^{17}O^-/^{187}Re^{16}O_3{}^-$ and $^{187}Re^{16}O_2{}^{18}O^-/^{187}Re^{16}O_3{}^-$ measured on Re filaments (n = 8) loaded with only 5 μg each of La and Gd were used (Table 3). The means of $^{17}O/^{16}O$ and $^{18}O/^{16}O$ determined by this study were 0.0003913 and 0.002096, respectively (Fig. 1). These values are significantly higher than the values used by previous studies, e.g., $^{17}O/^{16}O$ = 0.0003749 and$^{18}O/^{16}O$ = 0.002044 [15,14,1]. Because $^{187}Re^{16}O_3{}^-$ is an isobar with $^{186}W^{16}O_2{}^{17}O^-$, measured $^{186}W^{16}O_2{}^{17}O^-/^{186}W^{16}O_3{}^-$ and $^{186}W^{16}O_2{}^{18}O^-/^{186}W^{16}O_3{}^-$ could not be used to make this estimate.

The repeated measurements of $^{187}Re^{16}O_2{}^{17}O^-/^{187}Re^{16}O_3{}^-$ and $^{187}Re^{16}O_2{}^{18}O^-/^{187}Re^{16}O_3{}^-$ from Re filaments also provides an oxygen mass fractionation line that is consistent with recently reported oxygen mass fractionation lines for $OsO_3{}^-$, $RuO_3{}^-$, and $MoO_3{}^-$ (Fig. 1) measured by N-TIMS [20–23]. These lines are all offset from the oxygen fractionation line used by previous W studies utilizing N-TIMS. The slope of a linear regression through the $ReO_3{}^-$ oxygen mass fractionation line (0.0985 ± 0.0018 2SD) is similar to the slope of the terrestrial fractionation line (0.0954), so the terrestrial fractionation slope was used to infer $^{17}O/^{16}O$ from measured $^{18}O/^{16}O$.

3.2. External and internal precision

The external precision (n = 6) of 300 ng–1000 ng *Alfa Aesar* W standards analyzed in February 2016 was 4.0 ppm and 3.6 ppm for$^{182}W/^{184}W$ normalized to $^{186}W/^{184}W$ ($^{182}W/^{184}W_{N6/4}$) and $^{186}W/^{183}W$ ($^{182}W/^{184}W_{N6/3}$), respectively (Table 4; Figs. 2 and 3). After Faraday cup maintenance (mechanical removal of deposits on graphite inserts from each Faraday cup, except the center cup) was performed in April 2016, the mean $^{182}W/^{184}W_{N6/4}$ shifted downwards by ~3 ppm (Fig. 2), whereas the $^{182}W/^{184}W_{N6/3}$ only shifted by ~1 ppm (Fig. 3). Faraday cup condition, therefore, appears to have a ~3x larger influence on $^{182}W/^{184}W_{N6/4}$ than $^{182}W/^{184}W_{N6/3}$.

The long-term external precision (n = 24; over a period of 3 months after Faraday cup maintenance) of 300 ng–1000 ng *Alfa Aesar* W standards analyzed from April-June 2016 was 5.7 ppm and 3.7 ppm for$^{182}W/^{184}W_{N6/4}$ and $^{182}W/^{184}W_{N6/3}$, respectively (Table 4; Figs. 2 and 3), which is 2–3 x more precise for $^{182}W/^{184}W_{N6/4}$ and $^{182}W/^{184}W_{N6/3}$ than the most recently reported method for measuring W via N-TIMS [1]. These improvements in precision are likely the result of the more accurate oxide corrections for both $WO_3{}^-$ and $ReO_3{}^-$. Consistent with prior studies [14,1], the long-term external precision of $^{182}W/^{184}W$ is better when normalizing to $^{186}W/^{183}W$ than $^{186}W/^{184}W$ because of the closer proximity of the normalizing isotopes (^{183}W vs. ^{184}W). However, normalization to $^{186}W/^{183}W$ is only appropriate for samples with $^{183}W/^{184}W$ identical to terrestrial standards, as ^{183}W varies among some meteorites. The long-term external precision of $^{182}W/^{184}W_{N6/4}$ and $^{182}W/^{184}W_{N6/3}$ were 5.2 ppm and 2.6 ppm, respectively, for thin ribbon (n = 11). For thick ribbon (n = 13), the $^{182}W/^{184}W_{N6/4}$ and $^{182}W/^{184}W_{N6/3}$ were 6.2 and 4.3 ppm, respectively.

The external precision of $^{183}W/^{184}W_{N6/4}$ for February 2016 was 4.3 ppm (Table 4; Fig. 4). $^{183}W/^{184}W_{N6/4}$ is also sensitive to Faraday cup condition and shifted by ~5 ppm after cup maintenance was performed in April 2016. The long-term external precision (n = 24) of 300 ng–1000 ng *Alfa Aesar* W standards analyzed from April-June 2016 was 6.6 ppm for$^{183}W/$

$^{184}W_{N6/4}$ (Table 4; Fig. 4). The long-term external precision of $^{183}W/^{184}W_{N6/4}$ was 6.0 ppm for thin filaments (n = 11), and 6.5 ppm for thick filaments (n = 13).

The internal precisions of interspersed 300 ng, 500 ng, and 1000 ng *Alfa Aesar* W standards were similar (~4–5 ppm 2 standard error of the mean (SE) for $^{182}W/^{184}W_{N6/4}$) when the same signal intensity (~1 V on ^{184}W) was achieved for 600 integrations (Fig. 5). However, only 1000 ng W standards measured on thin Re ribbon achieved much greater than ~1 V on ^{184}W, and correspondingly better internal precision (~3 ppm 2SE for $^{182}W/^{184}W_{N6/4}$). The best internal precisions (average 2SE of 3.6 ppm) for $^{182}W/^{184}W$ were achieved by using $^{186}W/^{183}W$ for mass bias corrections. By contrast, the average of internal precisions of $^{182}W/^{184}W$ mass bias corrected using $^{186}W/^{184}W$ was 4.7 ppm 2SE. For $^{183}W/^{184}W$ mass bias corrected using $^{186}W/^{184}W$, the average internal precision was 4.2 ppm 2SE.

3.3. Measurements with high Re signals

Ref. [1] reported correlations between Re/W signals, $^{182}W/^{184}W$, and oxygen isotopic compositions. Because that study used the oxygen isotopic composition of atmosphere reported by [15] to calculate $^{17}O/^{16}O$ from measured $^{18}O/^{16}O$, corrections for species incorporating ^{17}O were too low, as the [15] isotopic composition deviates negatively in $^{17}O/^{16}O$ from the oxygen isotopic compositions measured during N-TIMS analyses and reported here (Fig. 1). Thus, the interference corrections for $^{187}Re^{17}O^{16}O_2$ on $^{186}W^{18}O^{16}O_2$ (which [1] used to determine $^{18}O/^{16}O$ and then calculate $^{17}O/^{16}O$) were too low. In this study, the use of more accurate $^{17}O/^{16}O$ removes this bias, and a correlation between Re/W signals and $^{182}W/^{184}W$ is not observed (Fig. 6).

3.4. Correlation of mass bias corrected ratios

Within the standards data reported by this study, a correlation exists between $^{182}W/^{184}W_{N6/4}$ and $^{183}W/^{184}W_{N6/4}$ (Fig. 7). A linear regression through the 30 measured standards using ISO-PLOT [24] has a slope of 1.41 ± 0.53 (2σ) and a mean square weighted deviation (MSWD) of 0.5. Ref. [1] also observed a correlated drift in $^{182}W/^{184}W_{N6/4}$ and $^{183}W/^{184}W_{N6/4}$ over a 9 month period. Among other possibilities, they stated that this could be the result of Faraday cup degradation over time. Because of the correlated, pronounced shift in $^{182}W/^{184}W_{N6/4}$ and $^{183}W/^{184}W_{N6/4}$ after cup maintenance, we conclude that the most likely cause of the correlated shift is Faraday cup degradation.

3.5. Measurement of natural samples

The measurement of natural samples with previously reported $^{182}W/^{184}W$ and $^{183}W/^{184}W$ provides a means to assess the accuracy of this analytical method. Ref. [5] reported that the $^{182}W/^{184}W$ and $^{183}W/^{184}W$ of group IVB iron meteorite Skookum, measured using a multi collector-inductively coupled plasma mass spectrometer (MC-ICP-MS), were well resolved from terrestrial standards (Fig. 8). Isotopic deviations of samples from standards here are described in μ units, where μ^xW is the isotopic deviation in parts per million of $^xW/^{184}W$ from a terrestrial standard. The $\mu^{182}W_{6/4}$ (−334.8 ± 5.7 2SD) and $\mu^{183}W_{6/4}$ (12.7 ± 6.6 2SD) of Skookum reported here is identical, within uncertainty, to one of two W isotopic compositions for the sample ($\mu^{182}W_{6/4}$ = −330 ± 4 2SE, and $\mu^{183}W_{6/4}$ = 13 ± 4 2SE) reported by [5]. Further, the precision reported here is for a single measurement and is

defined as the 2SD long-term external precision of standards analyzed during this study. By contrast, the precision reported by [5] represents the 2SE (n = 5) of repeated measurements. Thus, the datum reported here illustrates the accuracy and precision of single measurements using this new analytical method.

4. Conclusions

We have refined recently reported N-TIMS techniques [14,1] to measure WO_3^- and determine $^{182}W/^{184}W$ and $^{183}W/^{184}W$ to high-precision. Most significantly, this technique makes more accurate first-order and per-integration oxide corrections to primary $^{x}WO_3^-$ signals by (i) utilizing updated values for $^{17}O/^{16}O$ and $^{18}O/^{16}O$ for first-order corrections, (ii) measuring $^{18}O/^{16}O$ for both WO_3^- and ReO_3^-, and (iii) using a new oxide mass fractionation line to calculate per-integration $^{17}O/^{16}O$ from measured $^{18}O/^{16}O$. The long-term external precisions for $^{182}W/^{184}W_{N6/4}$, $^{182}W/^{184}W_{N6/3}$, and $^{183}W/^{184}W_{N6/4}$ are 5.7 ppm, 3.7 ppm, and 6.6 ppm, respectively. This level of precision is ~2–3 x better for single measurements than the most recently reported N-TIMS method for measuring both $^{182}W/^{184}W$ and $^{183}W/^{184}W$ [1]. We have demonstrated that this method is capable of producing accurate and precise data for natural samples by using this method to measure a group IVB iron meteorite, and comparing the datum to previously reported data for this sample [5].

Acknowledgements

This work was supported by NASA Cosmochemistry grant NNX13AF83G. We would like to thank Anne Trinquier and Nick Sharp for analytical advice and helpful discussions. We would also like to thank James Farquhar and Ed Young for providing insights into oxygen isotope fractionation. Igor Puchtel and Mathieu Touboul are thanked for their help in the lab. Two anonymous reviewers provided feedback, and helped improve the quality of the manuscript. We thank our editor, Perdita Barran.

References

[1]. Trinquier A, Touboul M, Walker RJ, High-precision tungsten isotopic analysis by multicollection negative thermal ionization mass spectrometry based on simultaneous measurement of W and $^{18}O/^{16}O$ isotope ratios for accurate fractionation correction, Anal. Chem 88 (2016) 1542–1546. [PubMed: 26751903]

[2]. Vockenhuber C, Oberli F, Bichler M, Ahmad I, Quitté G, Meier M, Halliday AN, Lee DC, Kutschera W, Steier P, Gehrke RJ, Helmer RG, New half-life measurement of ^{182}Hf: improved chronometer for the early solar system, Phys. Rev. Lett 93 (2004) 172501. [PubMed: 15525068]

[3]. Lee DC, Halliday AN, Hafnium–tungsten chronometry and the timing of terrestrial core formation, Nature 378 (1995) 771–774.

[4]. Harper CL, Jacobsen SB, Evidence for ^{182}Hf in the early Solar System and constraints on the timescale of terrestrial accretion and core formation, Geochim. Cosmochim. Acta 60 (1996) 1131–1153.

[5]. Kruijer TS, Touboul M, Fischer-Godde M, Bermingham KR, Walker RJ, Kleine T, Protracted core formation and rapid accretion of protoplanets, Science 344 (2014) 1150–1154. [PubMed: 24904163]

[6]. Kleine T, Touboul M, Van Orman JA, Bourdon B, Maden C, Mezger K, Halliday A, Hf–W thermochronometry: closure temperature and constraints on the accretion and cooling history of the H chondrite parent body, Earth Planet. Sci. Lett 270 (2008) 106–118.

[7]. Kruijer TS, Kleine T, Fischer-Gödde M, Burkhardt C, Wieler R, Nucleosynthetic W isotope anomalies and the Hf-W chronometry of Ca-Al-rich inclusions, Earth Planet. Sci. Lett 403 (2014) 317–327.

[8]. Budde G, Kleine T, Kruijer TS, Burkhardt C, Metzler K, Tungsten isotopic constraints on the age and origin of chondrules, Proc. Natl. Acad. Sci. U. S. A 113 (2016) 2886–2891. [PubMed: 26929340]

[9]. Willbold M, Elliott T, Moorbath S, The tungsten isotopic composition of the Earth's mantle before the terminal bombardment, Nature 477 (2011) 195–198. [PubMed: 21901010]

[10]. Willbold M, Mojzsis SJ, Chen H-W, Elliott T, Tungsten isotope composition of the Acasta Gneiss complex, Earth Planet. Sci. Lett 419 (2015) 168–177.

[11]. Touboul M, Puchtel IS, Walker RJ, ^{182}W evidence for long-term preservation of early mantle differentiation products, Science 335 (2012) 1065–1069. [PubMed: 22345398]

[12]. Touboul M, Liu J, O'Neil J, Puchtel IS, Walker RJ, New insights into the Hadean mantle revealed by ^{182}Wand highly siderophile element abundances of supracrustal rocks from the Nuvvuagittuq Greenstone Belt Quebec, Canada, Chem. Geol 383 (2014) 63–75.

[13]. Liu J, Touboul M, Ishikawa A, Walker RJ, Pearson DG, Widespread tungsten isotope anomalies and W mobility in crustal and mantle rocks of the Eoarchean Saglek Block, northern Labrador, Canada : Implications for early Earth processes and W recycling, Earth Planet. Sci. Lett 448 (2016) 12–23.

[14]. Touboul M, Walker RJ, High precision measurement of tungsten isotopes by thermal ionization mass spectrometry, Int. J. Mass Spectrom 309 (2012) 109–117.

[15]. Nier AO, A redetermination of the relative abundances of the isotopes of carbon, nitrogen, oxygen, argon, and potassium, Phys. Rev 77 (1950) 789–793.

[16]. Clayton RN, Oxygen isotopes in meteorites, Ann. Rev. Earth Planet. Sci 21 (1993) 115–149.

[17]. Yin QZ, N-TIMS Technique for the Re-Os and Ru Isotopic Systems and Its Application to Selected Geochemical and Cosmochemical Problems. PhD Thesis, University of Mainz and Max Planck Institute for Chemistry, 1995.

[18]. Völkening J, Köppe M, Heumann KG, Tungsten isotope ratio determinations by negative thermal ionization mass spectrometry, Int. J. Mass Spectrom. Ion Processes 107 (1991) 361–368.

[19]. Russell WA, Papanastassiou DA, Tombrello TA, Ca isotope fractionation in the Earth and other solar system materials, Geochim. Cosmochim. Acta 42 (1978) 1075–1090.

[20]. Bermingham KR, Walker RJ, Worsham EA, Refinement of high precision Ru isotope analysis using negative thermal ionization mass spectrometry, Int. J. Mass Spectrom 403 (2016) 15–26.

[21]. Worsham EA, Walker RJ, Bermingham KR, High-precision molybdenum isotope analysis by negative thermal ionization mass spectrometry, Int. J. Mass Spectrom 407 (2016) 51–61.

[22]. Chu Z-Y, Li C-F, Chen Z, Xu J-J, Di Y-K, Guo J-H, High-precision measurement of ^{186}Os/^{188}Os and ^{187}Os/^{188}Os: isobaric oxide corrections with in-run measured oxygen isotope ratios, Anal. Chem 87 (2015) 8765–8771. [PubMed: 26255581]

[23]. Nagai Y, Yokoyama T, Molybdenum isotopic analysis by negative thermal ionization mass spectrometry (N-TIMS): Effects on oxygen isotopic composition, J. Anal. At. Spectrom 29 (2016) 1090–1096.

[24]. Ludwig KR, Users Manual for Isoplot/Ex Version 2 47. A Geochronological Toolkit for Microsoft Excel, Berkeley Geochronology Center Special Publication 1a, 2001, pp. 55.

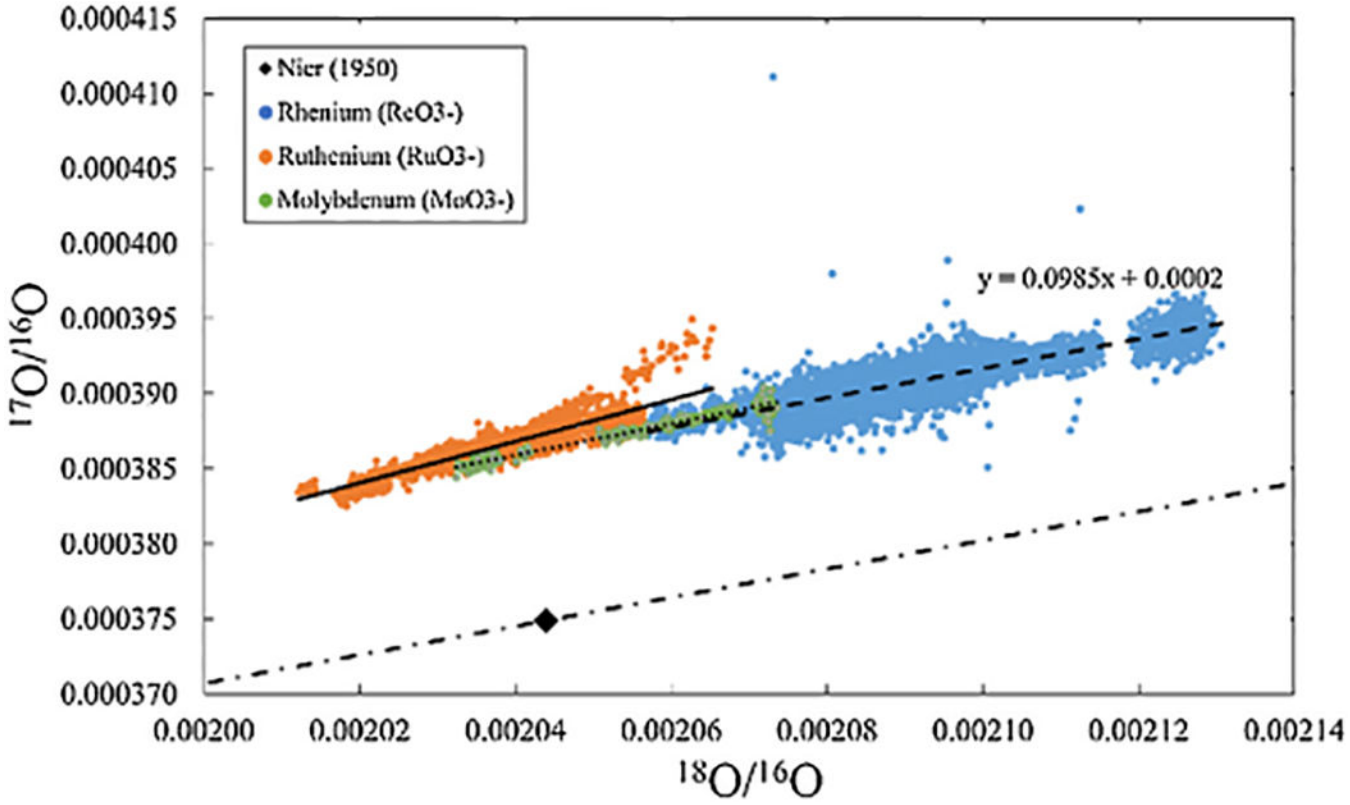

Fig. 1.

Measured oxygen isotopic compositions for ReO_3^- (this study), RuO_3^- [20], and MoO_3^- [21]. The oxygen isotopic composition of atmosphere reported by Nier (1950) and a terrestrial fractionation line (dashed-dotted line), which were used by previous studies [14,1] are shown for reference. Linear regressions are shown as dashed (ReO_3^-), solid (RuO_3^-), and dotted (MoO_3^-) lines.

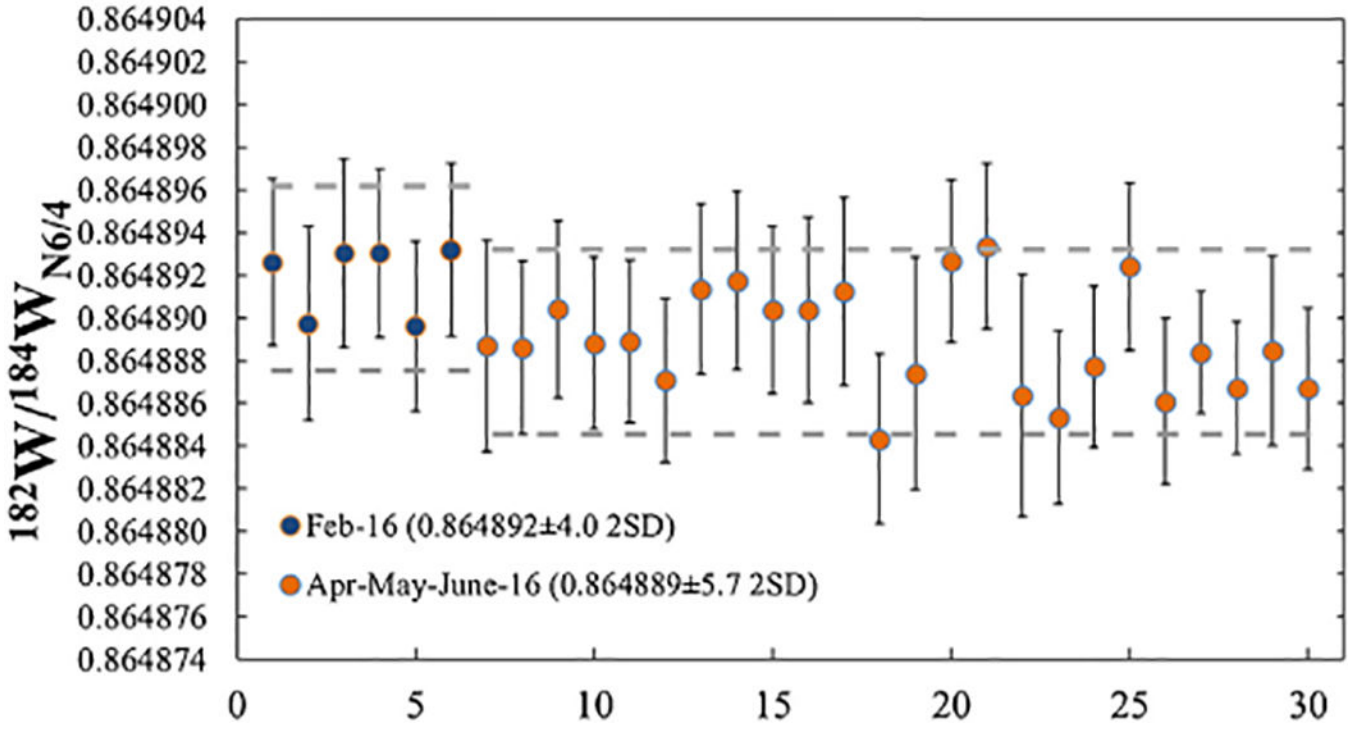

Fig. 2.

$^{182}W/^{184}W$ normalized to $^{186}W/^{184}W$ for 30 analyses of 300ng–1000 ng *Alfa Aesar* W standards. Mean $^{182}W/^{184}W$ and 2SD for each period shown in legend. Grey dashed lines mark 5 ppm from the mean. Error bars represent 2SE internal precisions.

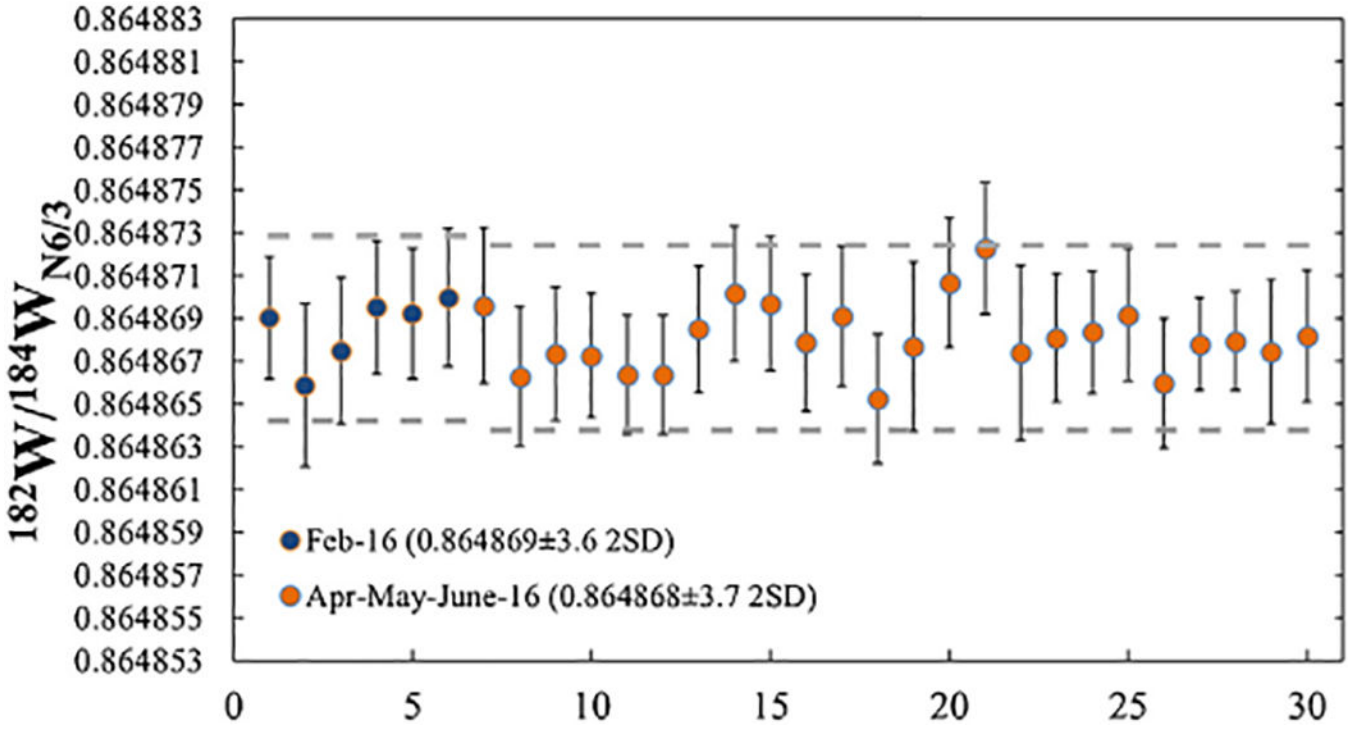

Fig. 3.

$^{182}W/^{184}W$ normalized to $^{186}W/^{183}W$ for 30 analyses of 300ng–1000 ng *Alfa Aesar* W standards. Mean $^{182}W/^{184}W$ and 2SD for each period shown in legend. Grey dashed lines mark 5 ppm from the mean. Error bars represent 2SE internal precisions.

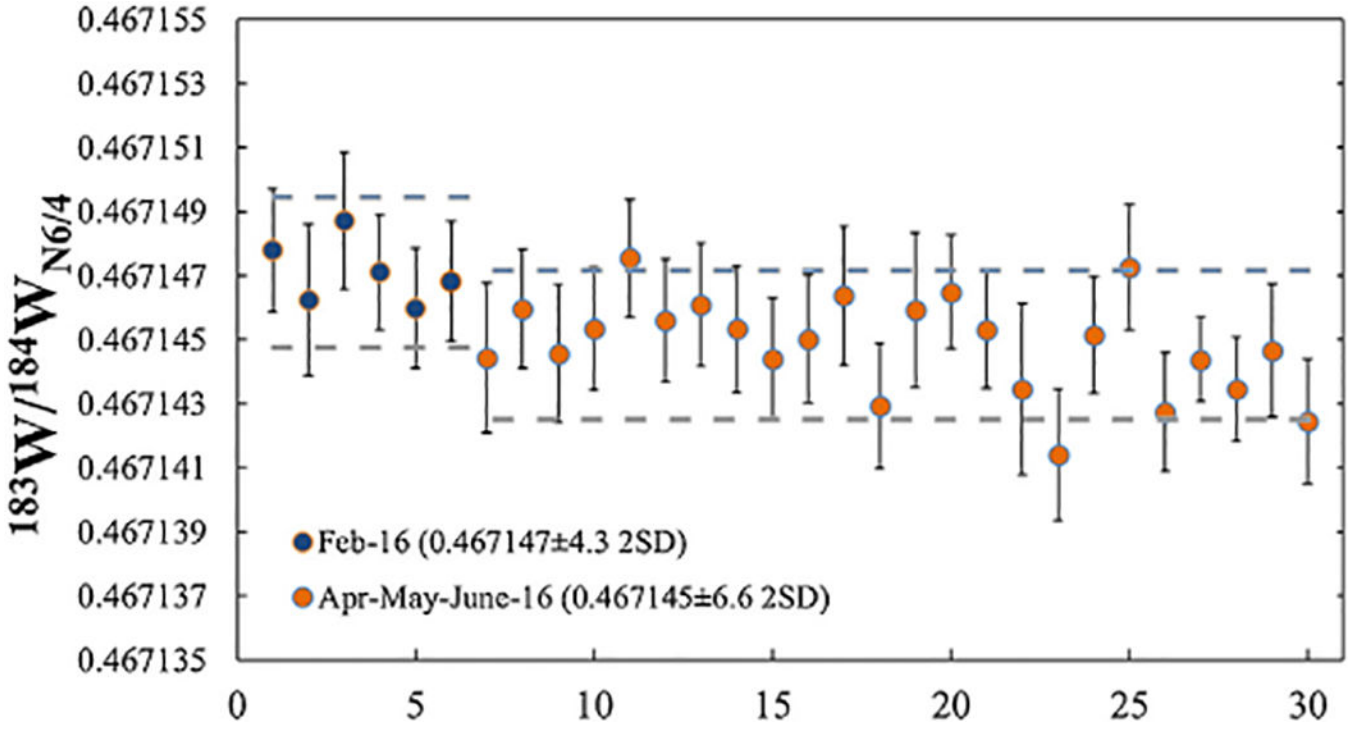

Fig. 4.

$^{183}W/^{184}W$ normalized to $^{186}W/^{184}W$ for 30 analyses of 300ng–1000 ng *Alfa Aesar* W standards. Mean $^{183}W/^{184}W$ and 2SD for each period shown in legend. Grey dashed lines mark 5 ppm from the mean. Error bars represent 2SE internal precisions.

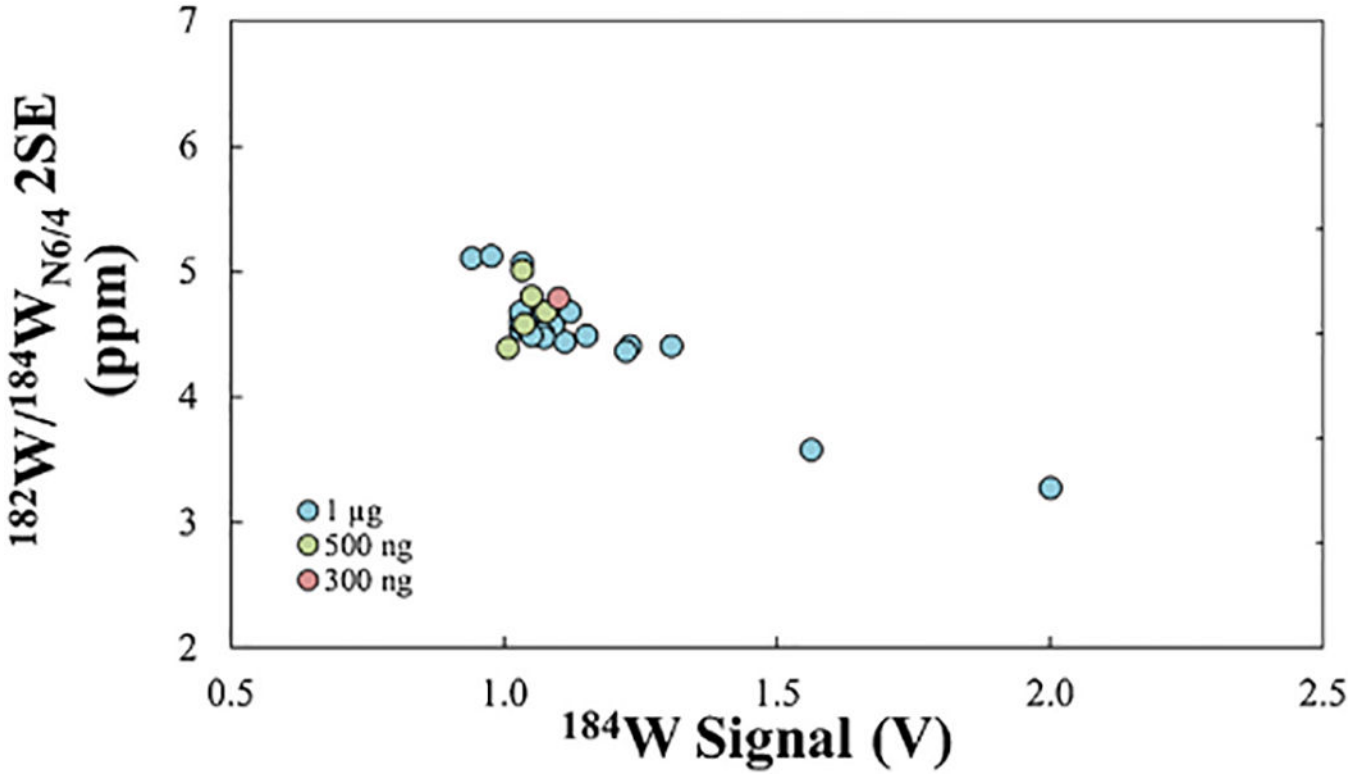

Fig. 5.

Average ^{184}W signal (volts) during analyses vs. the internal precision (2SE) for $^{182}W/^{184}W$ (normalized to $^{186}W/^{184}W$) of 26 analyses of 300ng–1000 ng *Alfa Aesar* W standards that were measured for 600 integrations. Analyses of both thick and thin filaments are included. Analyses that were measured for fewer than 600 integrations are not included.

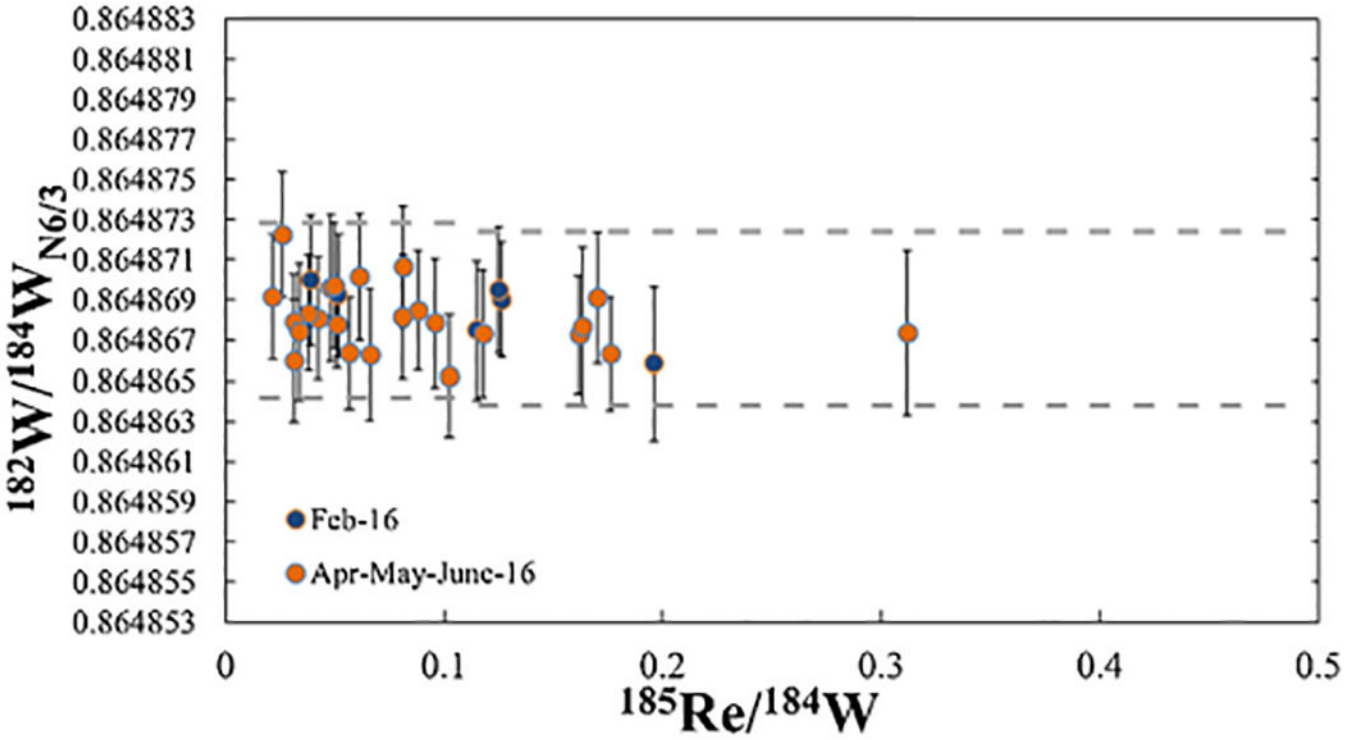

Fig. 6.

Mean $^{185}Re/^{184}W$ (for each measurement) vs. $^{182}W/^{184}W$ (normalized to $^{186}W/^{183}W$) for 30 analyses of 300ng–1000 ng *Alfa Aesar* W standards. Grey dashed lines mark 5 ppm from the mean. Error bars represent 2SE internal precisions.

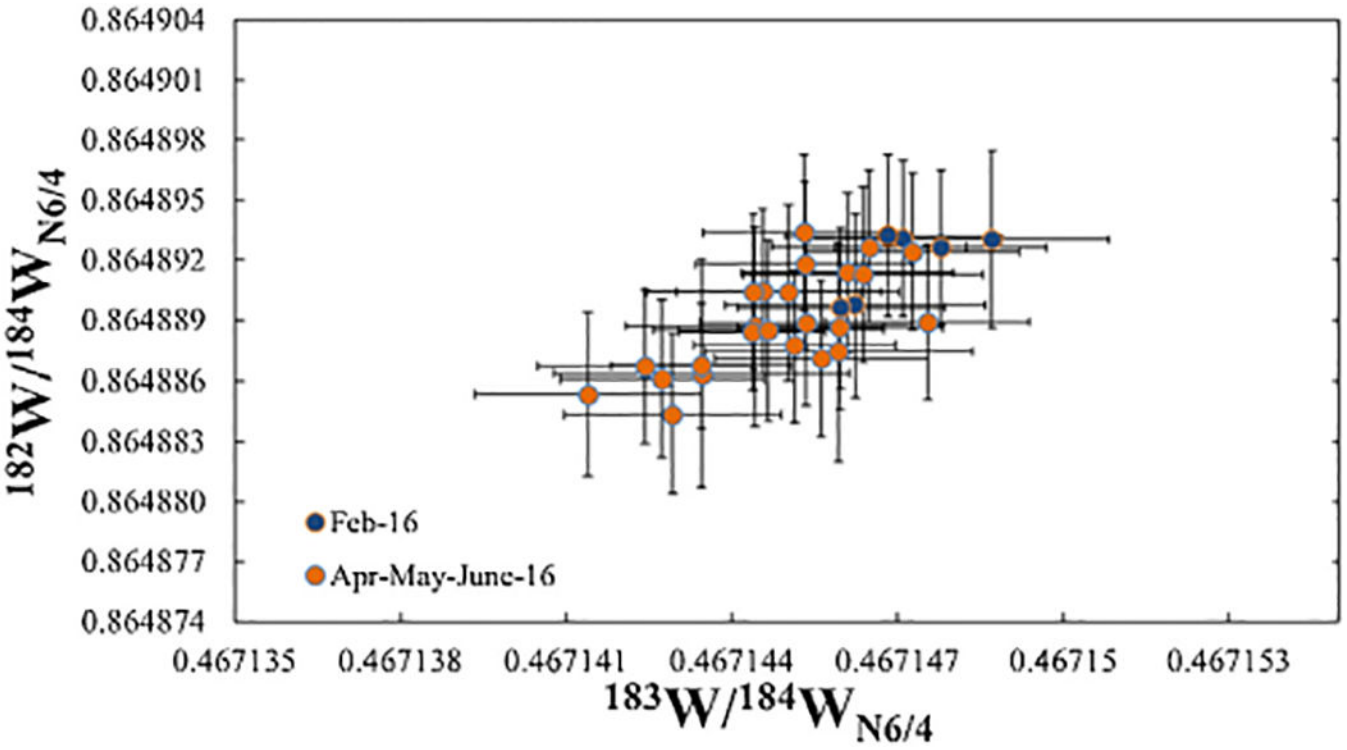

Fig. 7.

$^{183}W/^{184}W_{N6/4}$ vs. $^{182}W/^{184}W_{N6/4}$ for 30 analyses of 300ng–1000 ng *Alfa Aesar* W standards. Error bars represent 2SE internal precisions.

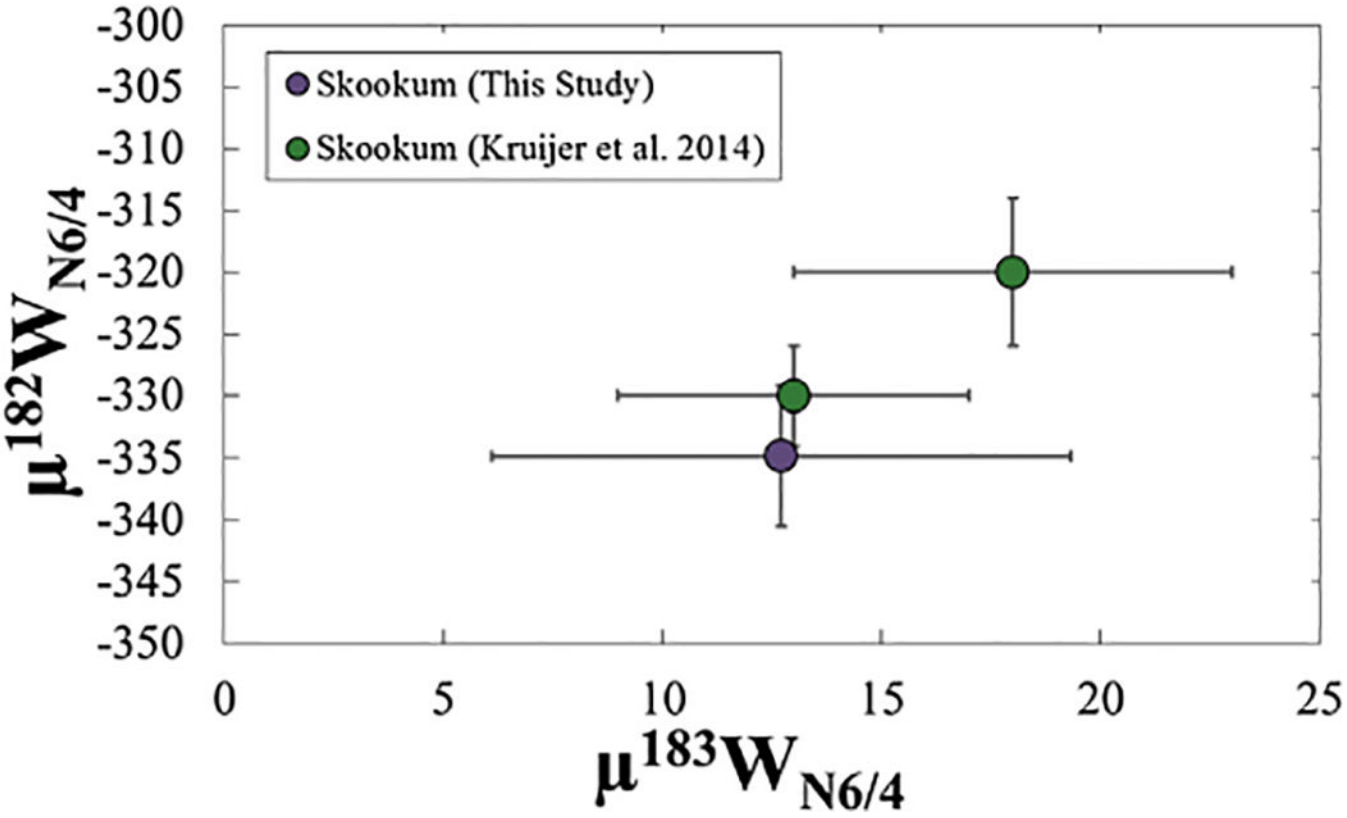

Fig. 8.

$\mu^{183}W_{N6/4}$ vs. $\mu^{182}W_{N6/4}$ for the group IVB iron meteorite Skookum. One analysis is from this study, and two analyses were taken from [5]. The error bars for the datum from this study are 2SD, and the error bars for the data from [5] are 2SE (n = 5) of repeated measurements.

Table 1

Faraday cup-amplifier-resistor configuration for measurement of W using N-TIMS utilizing 9 Faraday cups.

	L4	L3	L2	L1	C	H1	H2	H3	H4
Line 1	$^{180}W^{16}O_3$	$^{181}Ta^{16}Oa$	$^{182}W^{16}O_3$	$^{183}W^{16}O_3$	$^{184}W^{16}O_3$	$^{185}Re^{16}O3$	$^{186}W^{16}O_3$	$^{186}W^{16}O_2{}^{18}O$	$^{187}Re^{16}O_2{}^{18}O$
Line 2	$^{182}W^{16}O_3$	$^{183}W^{16}O_3$	$^{184}W^{16}O_3$	$^{185}Re^{16}O_3$	$^{186}W^{16}O_3$	$^{187}Re^{16}O_3$	$^{186}W^{16}O_2{}^{18}O$	$^{190}Os^{16}O_3$	
Resistor	$10^{11}\ \Omega$	$10^{11}\ \Omega$	$10^{11}\ \Omega$	$10^{11}\ \Omega$	$10^{11}\ \Omega$	$10^{11}\ \Omega$	$10^{11}\ \Omega$	$10^{12}\ \Omega$	$10^{12}\ \Omega$

Table 2

Interferences on primary $x^{16}O_3^-$ species that require corrections. Oxygen isotopic compositions represent total oxygen masses (e.g., $^{184}W^{50}O_3^-$ = $^{184}W^{16}O_2{}^{18}O^-$ + $^{184}W^{16}O^{17}O_2^-$).

Species	**$^{180}W^{16}O_3^-$**	**$^{182}W^{16}O_3^-$**	**$^{183}W^{16}O_3^-$**	**$^{184}W^{16}O_3^-$**	**$^{185}Re^{16}O_3^-$**	**$^{186}W^{16}O_3^-$**	**$^{187}Re^{16}O_3^-$**	**$^{186}W^{16}O_2{}^{18}0^-$**	**$^{187}Re^{16}O_2{}^{18}O^-$**
Mass	228	230	231	232	233	234	235	236	237
	$^{180}Ta^{48}O_3^-$	$^{180}W^{50}O_3^-$	$^{180}W^{51}O_3^-$	$^{180}W^{52}O_3^-$	$^{181}Ta^{52}O_3^-$	$^{182}W^{52}O_3^-$	$^{183}W^{52}O_3^-$	$^{184}W^{52}O_3^-$	$^{185}Re^{52}O_3^-$
Interfering		$^{180}Ta^{50}O_3^-$	$^{180}Ta^{51}O_3^-$	$^{180}Ta^{52}O_3^-$	$^{182}W^{51}O_3^-$	$^{183}W^{51}O_3^-$	$^{184}W^{51}O_3^-$	$^{185}Re^{51}O_3^-$	$^{186}W^{51}O_3^-$
Species		$^{181}Ta^{49}O_3^-$	$^{181}Ta^{50}O_3^-$	$^{181}Ta^{51}O_3^-$	$^{183}w^{50}O_3^-$	$^{184}w^{50}O_3^-$	$^{185}Re^{50}O_3^-$	$^{187}Re^{49}O_3^-$	
			$^{182}w^{49}O_3^-$	$^{182}W^{50}O_3^-$	$^{184}w^{49}O_3^-$	$^{185}Re^{49}O_3^-$	$^{186}w^{49}O_3^-$		
				$^{183}w^{49}O_3^-$					

Table 3

Data for 8 analyses of Re ribbon with only activator (5 μg each La and Gd loaded). Errors are 2SD internal precisions and reflect in-run evolution of oxygen isotopic compositions.

Analysis #	$^{18}O/^{16}O$	2SD (‰)	$^{17}O/^{16}O$	2SD (‰)
1	0.002085	5.4	0.0003894	6.2
2	0.002090	7.6	0.0003905	7.1
3	0.002100	2.6	0.0003917	3.8
4	0.002110	2.9	0.0003926	3.9
5	0.002125	2.3	0.0003940	4.7
6	0.002098	4.1	0.0003919	3.8
7	0.002088	8.1	0.0003906	9.1
8	0.002074	8.1	0.0003896	5.7
Mean	0.002096	7.7‰	0.0003913	4.1 ‰

Table 4

Standards data for 30 analyses of 300 ng–1000 ng of *Alfa Aesar* W. Errors are 2SE absolute internal precisions. $^{185}Re/^{184}W$ are the average signal intensity ratios for entire analyses.

Standard #	Session ID #	W Abundance	Type	Date	$^{185}Re/^{184}W$	$^{182}W/^{184}W_{N6/4}$	2SE	$^{183}W/^{184}W_{N6/4}$	2SE	$^{182}W/^{184}W_{N6/3}$	2SE
1	381	1 μg	Thick	Feb 18, 2016	0.126	0.864893	0.000004	0.467148	0.000002	0.864869	0.000003
2	381	300 ng	Thick	Feb 19, 2016	0.196	0.864890	0.000005	0.467146	0.000002	0.864866	0.000004
3	382	1 μg	Thick	Feb 24, 2016	0.115	0.864893	0.000004	0.467149	0.000002	0.864867	0.000003
4	382	1 μg	Thick	Feb 25, 2016	0.125	0.864893	0.000004	0.467147	0.000002	0.864870	0.000003
5	382	1 μg	Thick	Feb 29, 2016	0.052	0.864890	0.000004	0.467146	0.000002	0.864869	0.000003
6	382	1 μg	Thick	March 3, 2016	0.039	0.864893	0.000004	0.467147	0.000002	0.864870	0.000003
Cup Maintenance Performed				April 1st, 2016	Mean 2SD(ppm)	0.864892 4.0		0.467147 4.3		0.864869 3.6	
7	385	1 μg	Thin	April 5, 2016	0.048	0.864889	0.000005	0.467144	0.000002	0.864870	0.000004
8	385	1 μg	Thick	April 6, 2016	0.066	0.864889	0.000004	0.467146	0.000002	0.864866	0.000003
9	385	300 ng	Thick	April 7, 2016	0.118	0.864890	0.000004	0.467145	0.000002	0.864867	0.000003
10	386	1 μg	Thick	April 11, 2016	0.162	0.864889	0.000004	0.467145	0.000002	0.864867	0.000003
11	386	1 μg	Thick	April 12, 2016	0.176	0.864889	0.000004	0.467148	0.000002	0.864866	0.000003
12	386	1 μg	Thick	April 13, 2016	0.057	0.864887	0.000004	0.467146	0.000002	0.864866	0.000003
13	386	1 μg	Thick	April 13, 2016	0.088	0.864891	0.000004	0.467146	0.000002	0.864868	0.000003
14	386	500 ng	Thin	April 14, 2016	0.061	0.864892	0.000004	0.467145	0.000002	0.864870	0.000003
15	386	1 μg	Thin	April 18, 2016	0.050	0.864890	0.000004	0.467144	0.000002	0.864870	0.000003
16	386	500 ng	Thin	April 19, 2016	0.096	0.864890	0.000004	0.467145	0.000002	0.864868	0.000003
17	386	1 μg	Thick	April 19, 2016	0.170	0.864891	0.000004	0.467146	0.000002	0.864869	0.000003
18	386	500 ng	Thick	April 20, 2016	0.102	0.864884	0.000004	0.467143	0.000002	0.864865	0.000003
19	386	500 ng	Thick	April 21, 2016	0.164	0.864887	0.000005	0.467146	0.000002	0.864868	0.000004
20	387	1 μg	Thin	April 25, 2016	0.081	0.864893	0.000004	0.467146	0.000002	0.864871	0.000003
21	387	1 μg	Thick	May 1, 2016	0.026	0.864893	0.000004	0.467145	0.000002	0.864872	0.000003
22	387	500 ng	Thick	May 2, 2016	0.312	0.864886	0.000006	0.467143	0.000003	0.864867	0.000004
23	389	500 ng	Thin	May 16, 2016	0.042	0.864885	0.000004	0.467141	0.000002	0.864868	0.000003
24	389	1 μg	Thin	May 17, 2016	0.038	0.864888	0.000004	0.467145	0.000002	0.864868	0.000003
25	389	1 μg	Thick	May 20, 2016	0.022	0.864892	0.000004	0.467147	0.000002	0.864869	0.000003
26	389	1 μg	Thick	May 22, 2016	0.031	0.864886	0.000004	0.467143	0.000002	0.864866	0.000003

Standard #	Session ID #	W Abundance	Type	Date	$^{185}Re/^{184}W$	$^{182}W/^{184}W_{N6/4}$	2SE	$^{183}W/^{184}W_{N6/4}$	2SE	$^{182}W/^{184}W_{N6/3}$	2SE
27	390	1 μg	Thin	May 26, 2016	0.051	0.864888	0.000003	0.467144	0.000001	0.864868	0.000002
28	390	1 μg	Thin	May 27, 2016	0.031	0.864887	0.000003	0.467143	0.000002	0.864868	0.000002
29	390	1 μg	Thin	May 30, 2016	0.034	0.864888	0.000004	0.467145	0.000002	0.864867	0.000003
30	390	500 ng	Thin	June 2, 2016	0.081	0.864887	0.000004	0.467142	0.000002	0.864868	0.000003
					Mean	0.864889		0.467145		0.864868	
					2SD (ppm)	5.7		6.6		3.7	